
Article:
Ohkitani, K. (2012) Asymptotics and numerics of a family of two-dimensional generalized surface quasi-geostrophic equations. Physics of Fluids, 24 (9). 095101. ISSN: 1070-6631

https://doi.org/10.1063/1.4748350

Asymptotics and numerics of a family of two-dimensional generalized surface quasi-geostrophic equations

Koji Ohkitani*

School of Mathematics and Statistics, University of Sheffield,

Hicks Building, Hounsfield Road, Sheffield S3 7RH, U.K.

(Dated: February 27, 2012)

Abstract

We study the generalised 2D surface quasi-geostrophic (SQG) equation, where the active scalar is given by a fractional power α of Laplacian applied to the stream function. This includes the 2D SQG and Euler equations as special cases.

Using Poincaré's successive approximation to higher α-derivatives of the active scalar, we derive a variational equation for describing perturbations in the generalized SQG equation. In particular, in the limit $\alpha \to 0$, an asymptotic equation is derived on a stretched time variable $\tau = \alpha t$, which unifies equations in the family near $\alpha = 0$. The successive approximation is also discussed at the other extreme of the 2D Euler limit $\alpha = 2$-0. Numerical experiments are presented for both limits.

We consider whether the solution becomes more singular or regular with increasing α. Two competing effects are identified: the regularizing effect of inverse "Laplacian" and cancellation by symmetry (nonlinearity depletion). Near $\alpha = 0$ (complete depletion) as α increases the solution becomes more singular. Near $\alpha = 2$ (maximal smoothing effect of inverse Laplacian) as α decreases the solution becomes more singular, suggesting that there may be some α in $[0, 1]$ at which the solution is most singular.

We also present some numerical results of the family for $\alpha = 0.5, 1$ and 1.5. On the original time t, the H_1 norm of θ generally grows more rapidly with increasing α. However, on the new time τ, this order is reversed. On the other hand, contour patterns for different α appear to be similar at fixed τ, even though the norms are markedly different in magnitude. Finally, point-vortex systems for the generalized SQG family are discussed to shed light on the above problems of time scale.

PACS numbers: Valid PACS appear here

*Electronic address: K.Ohkitani@sheffield.ac.uk

I. INTRODUCTION

The surface quasi-geostrophic (SQG, hereafter) equation has been attracting attention of many mathematical researchers since the appearance of the seminal papers [1, 2]. Since then, lots of studies have been made both mathematically and computationally, e.g. [3–11]. In this paper we consider a class of generalised SQG equations [12–16]. While only the 2D Euler and the SQG equation are physically relevant, considering more general cases helps understanding the genuine SQG equation. In spite of mathematical progress in the analysis of the SQG equation, the results are not completely satisfactory for ideal fluids, that is, while we know the global regularity for 2D Euler equations ($\alpha = 2$), global regularity for the rest of the family is not known. For hypo-viscous fluids, global regularity is known for critical and sub-critical cases [10, 11],

Here, an attempt is made to describe the behaviour of the family systematically. We will develop a perturbation theory, which suggests an introduction of a new stretched time variable and an asymptotic equation will then be derived and discussed on this basis.

The rest of this paper is organized as follows. In section II, a mathematical formulation of the generalized SQG equation is given. In Section III, a perturbation scheme with respect to the parameter α is described. In Section IV, asymptotic analyses are given for the limits $\alpha \to 0$ and $\alpha \to 2$, followed by some numerical results. In section V, numerical results for other values of α are presented. Finally, section VI is devoted to summary and outlook.

II. MATHEMATICAL FORMULATION

A. Governing equations

For an incompressible velocity field $\boldsymbol{u} = \nabla^{\perp}\psi$ in two dimensions, the generalized SQG equation is written as

$$\frac{\partial \theta}{\partial t} + \boldsymbol{u} \cdot \nabla \theta = 0, \tag{1}$$

where $\nabla^{\perp} = (\partial_y, -\partial_x)$ is a skew gradient and the active scalar θ is related to the stream function ψ by

$$\theta = \Lambda^{\alpha}\psi. \tag{2}$$

Here $\Lambda = (-\triangle)^{1/2}$ is the Zygmund operator defined as $|\boldsymbol{k}|$ by a Fourier transform, where $\boldsymbol{k}$ is the wavenumber. This system includes as special cases the 2D Euler equation ($\alpha = 2$)

$$\frac{\partial \omega}{\partial t} + \boldsymbol{u} \cdot \nabla \omega = 0, \tag{3}$$

$$\omega = -\triangle \psi \tag{4}$$

and the SQG equations ($\alpha = 1$)

$$\frac{\partial \theta}{\partial t} + \boldsymbol{u} \cdot \nabla \theta = 0, \tag{5}$$

$$\theta = (-\triangle)^{1/2} \psi. \tag{6}$$

The case with $\alpha = 0$ defines a steady equation $\dfrac{\partial \theta}{\partial t} = 0$. Note that the case $\alpha \to 0$ can be regarded as the Charney-Hasegawa-Miwa equation, e.g. [17]

$$\frac{\partial q}{\partial t} + (\boldsymbol{u} \cdot \nabla) q = 0, \ q = (\lambda^2 - \triangle)\psi,$$

in the limit of large Rossby deformation radius $\lambda \to \infty$, where q is the potential vorticity.

We will begin by considering the following question: *As we change α, the property of the solution to the generalized system changes. Does the solution become more regular or singular with increasing α ?* In fact, this question has turned out to be non-trivial because there are at least two competing factors in the problem.

To see this, let us consider the governing equation for $\theta(\boldsymbol{k})$ in Fourier space

$$\frac{\partial \theta(\boldsymbol{k})}{\partial t} = \sum_{\boldsymbol{k}=\boldsymbol{p}+\boldsymbol{q}} \frac{\boldsymbol{p} \times \boldsymbol{q}}{|\boldsymbol{q}|^{\alpha}} \theta(\boldsymbol{p}) \theta(\boldsymbol{q}), \tag{7}$$

which has two invariants of motion

$$Q = \frac{1}{2} \sum_{\boldsymbol{k}} |\theta(\boldsymbol{k})|^2 \text{ and } H_{\alpha} = \frac{1}{2} \sum_{\boldsymbol{k}} \frac{|\theta(\boldsymbol{k})|^2}{|\boldsymbol{k}|^{\alpha}}. \tag{8}$$

Hereafter, the zero mode $\boldsymbol{k} = 0$ should be discarded in the summation in Fourier space,

We make two observations regarding (7).

1) The parameter α appears as an exponent of the inverse Zygmund operator. This implies that the larger α is, the more regular integrand becomes, suggesting that the solution would behave in a more regular manner with increasing α.

The extreme limit $\alpha = 0$ corresponds to a trivial steady state by a cancellation effect due to symmetry (so-called nonlinearity depletion). In physical space, this is because the

advection term vanishes as a Jacobian determinant of the same functions. In wavenumber space, the nonlinear term vanishes because the convolution is anti-symmetric with respect to the exchange of $\boldsymbol{p}$ and $\boldsymbol{q}$.

2) By continuity, the motion is expected to be slow in the vicinity of $\alpha = 0$. In this neighborhood, with the increase of α from 0 this symmetry would be broken even further, suggesting a more singular behavior. We may recall a phenomenological argument [12] which indicates that $\alpha = 1$ may be the most 'dangerous' case of the family (see Appendix B for consideration using point vortices). These two effects are schematically shown in the parameter space Fig.1.

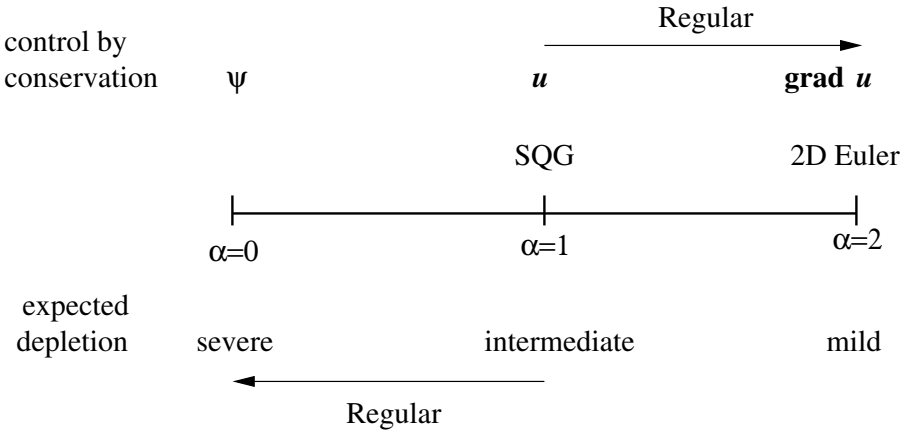

FIG. 1: Parameter space α: effects conservation and nonlinearity depletion.

III. PERTURBATION THEORY

A. Case of whole plane $\mathbb{R}^2$

We apply a classical perturbation theory to the SQG equation (see Appendix A). The first-order variation is obtained by taking a derivative of (1) with respect to α

$$\frac{\partial}{\partial t}\frac{\partial \theta}{\partial \alpha} + \boldsymbol{u}\cdot\nabla\frac{\partial \theta}{\partial \alpha} + \frac{\partial \boldsymbol{u}}{\partial \alpha}\cdot\nabla\theta = 0. \tag{9}$$

By using an integral expression for the Riesz potential, we can write

$$\boldsymbol{u} = \frac{1}{\gamma(\alpha)}\int \frac{\nabla^{\perp}\theta(\boldsymbol{y})}{|\boldsymbol{x}-\boldsymbol{y}|^{2-\alpha}}\mathrm{d}\boldsymbol{y}, \quad (0<\alpha<2), \tag{10}$$

where

$$\gamma(\alpha) = \frac{\pi 2^\alpha \Gamma(\alpha/2)}{\Gamma((2-\alpha)/2)}, \tag{11}$$

Γ is the gamma function and $\fint$ denotes a principal-value integral.

We consider the special limit $\alpha \to 2$. Noting that $\gamma(\alpha) \approx 2\pi(2-\alpha)$ as $\alpha \to 2$, we have by l'Hospital rule

$$\lim_{\alpha\to 2} \frac{r^{\alpha-2}}{\gamma(\alpha)} = \lim_{\alpha\to 2} \frac{r^{\alpha-2}\log r}{\gamma'(\alpha)} = \frac{1}{2\pi}\log\frac{1}{r},$$

which is nothing but the Green function for the 2D Laplacian. Similarly, we can check that

$$\begin{aligned}\frac{\partial}{\partial\alpha}\left(\frac{r^{\alpha-2}}{\gamma(\alpha)}\right) &= -\frac{\gamma'(\alpha)}{\gamma(\alpha)^2} r^{\alpha-2} + \frac{r^{\alpha-2}\log r}{\gamma(\alpha)} \\ &\to -\frac{1}{4\pi}\left(\log\frac{1}{r}\right)^2 \quad \text{as} \quad \alpha \to 2,\end{aligned}$$

by a repeated use of the similar operation. It follows in this limit that

$$\frac{\partial \boldsymbol{u}}{\partial\alpha} = -\frac{1}{4\pi}\int (\log|\boldsymbol{x}-\boldsymbol{y}|)^2 \nabla^\perp\omega(\boldsymbol{y})d\boldsymbol{y} + \frac{1}{2\pi}\int \log\frac{1}{|\boldsymbol{x}-\boldsymbol{y}|}\nabla^\perp\frac{\partial\omega(\boldsymbol{y})}{\partial\alpha}d\boldsymbol{y}. \tag{12}$$

Then, the leading-order variational equation near $\alpha = 2$ becomes

$$\frac{D}{Dt}\frac{\partial\omega}{\partial\alpha} = \frac{1}{2\pi}\int \frac{(\boldsymbol{x}-\boldsymbol{y})^\perp}{|\boldsymbol{x}-\boldsymbol{y}|^2}\frac{\partial\omega(\boldsymbol{y})}{\partial\alpha}d\boldsymbol{y}\cdot\nabla\omega + \frac{1}{4\pi}\int (\log|\boldsymbol{x}-\boldsymbol{y}|)^2\nabla^\perp\omega(\boldsymbol{y})d\boldsymbol{y}\cdot\nabla\omega. \tag{13}$$

In principle, higher-order derivatives can be worked out in a straightforward manner, but in practice the results are getting increasingly complicated.

B. Case of periodic boundary conditions

In the case of a flow under periodic boundary conditions, the analysis turns out to be much more tractable than the case of $\mathbb{R}^2$ because the α-dependence appears in one place in the dynamical equation. For example, let us write first two of higher derivatives. The first variation reads

$$\frac{\partial}{\partial t}\frac{\partial\theta(\boldsymbol{k})}{\partial\alpha} = \sum_{\boldsymbol{k}=\boldsymbol{p}+\boldsymbol{q}} \frac{\boldsymbol{p}\times\boldsymbol{q}}{|\boldsymbol{q}|^\alpha}\left(\frac{\partial\theta(\boldsymbol{p})}{\partial\alpha}\theta(\boldsymbol{q}) + \theta(\boldsymbol{p})\frac{\partial\theta(\boldsymbol{q})}{\partial\alpha} + \theta(\boldsymbol{p})\theta(\boldsymbol{q})\log\frac{1}{|\boldsymbol{q}|}\right), \tag{14}$$

whereas the second variation is given by

$$\begin{aligned}\frac{\partial}{\partial t}\frac{\partial^2\theta(\boldsymbol{k})}{\partial\alpha^2} = \sum_{\boldsymbol{k}=\boldsymbol{p}+\boldsymbol{q}} \frac{\boldsymbol{p}\times\boldsymbol{q}}{|\boldsymbol{q}|^\alpha}\Bigg[&\theta(\boldsymbol{p})\theta(\boldsymbol{q})\left(\log\frac{1}{|\boldsymbol{q}|}\right)^2 + 2\left(\frac{\partial\theta(\boldsymbol{p})}{\partial\alpha}\theta(\boldsymbol{q}) + \theta(\boldsymbol{p})\frac{\partial\theta(\boldsymbol{q})}{\partial\alpha}\right)\log\frac{1}{|\boldsymbol{q}|} \\ &+ \left(\frac{\partial^2\theta(\boldsymbol{p})}{\partial\alpha^2}\theta(\boldsymbol{q}) + 2\frac{\partial\theta(\boldsymbol{p})}{\partial\alpha}\frac{\partial\theta(\boldsymbol{q})}{\partial\alpha} + \theta(\boldsymbol{p})\frac{\partial^2\theta(\boldsymbol{q})}{\partial\alpha^2}\right)\Bigg].\end{aligned} \tag{15}$$

In general, we make use of binomial expansion to write

$$\frac{\partial}{\partial t}\frac{\partial^n \theta(\boldsymbol{k})}{\partial \alpha^n} = \sum_{r=0}^{n} \binom{n}{r} \sum_{\boldsymbol{k}=\boldsymbol{p}+\boldsymbol{q}} \frac{\boldsymbol{p}\times\boldsymbol{q}}{|\boldsymbol{q}|^\alpha} \left(\log\frac{1}{|\boldsymbol{q}|}\right)^{n-r} \sum_{s=0}^{r} \binom{r}{s} \frac{\partial^s \theta(\boldsymbol{p})}{\partial \alpha^s} \frac{\partial^{r-s}\theta(\boldsymbol{q})}{\partial \alpha^{r-s}}. \tag{16}$$

We may apply those variational equations for any α ($0 \le \alpha \le 2$) if we assume existence of solution at that α. There are two cases where global regularity is known: one is the case $\alpha = 2$ for the 2D Euler flows and the other is $\alpha = 0$ for a trivial steady solution. We treat the simpler case $\alpha = 0$ here in connection with asymptotics in that neighborhood and discuss the case $\alpha = 2$ using numerics later.

For $\alpha = 0$, all the $\theta(\cdot)$ that appear as the coefficients in the variational equations are constant. Hence the first-order equation is easily solved and we have

$$\frac{\partial \theta}{\partial \alpha} = C_{11}(\boldsymbol{k})t, \tag{17}$$

where

$$C_{11}(\boldsymbol{k}) = \sum_{\boldsymbol{k}=\boldsymbol{p}+\boldsymbol{q}} (\boldsymbol{p}\times\boldsymbol{q})\theta(\boldsymbol{p})\theta(\boldsymbol{q}) \log\frac{1}{|\boldsymbol{q}|}. \tag{18}$$

At the second-order, we find similarly

$$\frac{\partial^2 \theta}{\partial \alpha^2} = C_{22}(\boldsymbol{k})t^2 + C_{21}(\boldsymbol{k})t, \tag{19}$$

where

$$C_{21}(\boldsymbol{k}) = \sum_{\boldsymbol{k}=\boldsymbol{p}+\boldsymbol{q}} (\boldsymbol{p}\times\boldsymbol{q})\theta(\boldsymbol{p})\theta(\boldsymbol{q}) \left(\log\frac{1}{|\boldsymbol{q}|}\right)^2 \tag{20}$$

and

$$C_{22}(\boldsymbol{k}) = \sum_{\boldsymbol{k}=\boldsymbol{p}+\boldsymbol{q}} (\boldsymbol{p}\times\boldsymbol{q}) \left[C_{11}(\boldsymbol{p})\theta(\boldsymbol{q}) + \theta(\boldsymbol{p})C_{11}(\boldsymbol{q})\right] \log\frac{1}{|\boldsymbol{q}|}. \tag{21}$$

In general, we can solve

$$\frac{\partial}{\partial t}\frac{\partial^n \theta(\boldsymbol{k})}{\partial \alpha^n} = \sum_{r=0}^{n-1} \binom{n}{r} \sum_{\boldsymbol{k}=\boldsymbol{p}+\boldsymbol{q}} (\boldsymbol{p}\times\boldsymbol{q}) \left(\log\frac{1}{|\boldsymbol{q}|}\right)^{n-r} \sum_{s=0}^{r} \binom{r}{s} \frac{\partial^s \theta(\boldsymbol{p})}{\partial \alpha^s} \frac{\partial^{r-s}\theta(\boldsymbol{q})}{\partial \alpha^{r-s}} \tag{22}$$

successively by using a Taylor series expansion in time

$$\theta_n = \sum_{j=0}^{n} C_{nj}(\boldsymbol{k})t^j, \quad |t| < \rho_t. \tag{23}$$

It is readily shown that the coefficients satisfy a recursion relationship

$$jC_{nj}(\boldsymbol{k}) = \sum_{r=0}^{n-1} \binom{n}{r} \sum_{\boldsymbol{k}=\boldsymbol{p}+\boldsymbol{q}} (\boldsymbol{p}\times\boldsymbol{q}) \left(\log\frac{1}{|\boldsymbol{q}|}\right)^{n-r} \sum_{s=0}^{r} \binom{r}{s} \sum_{l=0}^{s} C_{sl}(\boldsymbol{p}) C_{r-s,j-1-l}(\boldsymbol{q}), \tag{24}$$

whose indices are constrained by $1 \le j \le n$ and $r \ge j-1$.

A formal perturbation series, which is a double series in t and α, now takes the form

$$\theta(\boldsymbol{k}, t, \alpha) = \theta(\boldsymbol{k}, t, 0) + \sum_{n=1}^{\infty} \alpha^n \theta_n(\boldsymbol{k}, t), \quad \text{for } |\alpha| < \rho_\alpha$$

and by (23)

$$= \theta(\boldsymbol{k}, t, 0) + \sum_{n=1}^{\infty} \sum_{j=0}^{n} \alpha^n t^j C_{nj}(\boldsymbol{k}) \quad \text{for } |t| < \rho_t, \tag{25}$$

where ρ_t, ρ_α are (unknown) radii of convergence. This suggests an introduction of a new variable $\tau \equiv \alpha t$ and we can write

$$\begin{aligned} \theta(\boldsymbol{k}, t, \alpha) &= \theta(\boldsymbol{k}, t, 0) + \sum_{n=1}^{\infty} \sum_{j=0}^{n} \tau^n t^{j-n} C_{nj}(\boldsymbol{k}) \\ &= \theta(\boldsymbol{k}, t, 0) + \sum_{n=1}^{\infty} \tau^n C_{nn}(\boldsymbol{k}) + \sum_{n=2}^{\infty} \sum_{j=1}^{n-1} t^{-(n-j)} C_{nj}(\boldsymbol{k}). \end{aligned} \tag{26}$$

within the radius of convergence $|\tau| < \rho_\alpha \rho_t$.

This expression suggests (but does not imply) a possibility of unifying equations in the family near $\alpha = 0$, because the residual term has negative powers in time and hence is expected to become small.

In passing we derive a simple recursion formula for the diagonal coefficients $A_n(\boldsymbol{k}) \equiv C_{nn}(\boldsymbol{k})$. Setting $j = n$ in (24), we have

$$nC_{nn}(\boldsymbol{k}) = \sum_{r=0}^{n-1} \binom{n}{r} \sum_{\boldsymbol{k}=\boldsymbol{p}+\boldsymbol{q}} (\boldsymbol{p} \times \boldsymbol{q}) \left(\log \frac{1}{|\boldsymbol{q}|} \right)^{n-r} \sum_{s=0}^{r} \binom{r}{s} \sum_{l=0}^{s} C_{sl}(\boldsymbol{p}) C_{r-s,n-1-l}(\boldsymbol{q}), \tag{27}$$

where only those terms with $r = n-1$ count. (The conditions on the indices $s \ge l \ge 0$ and $r - s \ge n - 1 - l$ imply $r \ge n-1$, whereas the range in the summation is $0 \le r \le n-1$.) It follows that

$$C_{nn}(\boldsymbol{k}) = \sum_{\boldsymbol{k}=\boldsymbol{p}+\boldsymbol{q}} (\boldsymbol{p} \times \boldsymbol{q}) \left(\log \frac{1}{|\boldsymbol{q}|} \right) \sum_{s=0}^{n-1} \binom{n-1}{s} \sum_{l=0}^{s} C_{sl}(\boldsymbol{p}) C_{n-1-s,n-1-l}(\boldsymbol{q}). \tag{28}$$

Again, by the conditions $s \ge l$ and $n-1-s \ge n-1-l$, only the term $s = l$ counts. We finally find

$$A_n(\boldsymbol{k}) = \sum_{\boldsymbol{k}=\boldsymbol{p}+\boldsymbol{q}} (\boldsymbol{p} \times \boldsymbol{q}) \left(\log \frac{1}{|\boldsymbol{q}|} \right) \sum_{s=0}^{n-1} \binom{n-1}{s} A_s(\boldsymbol{p}) A_{n-1-s}(\boldsymbol{q}), \tag{29}$$

where $A_0(\boldsymbol{k}) = \theta(\boldsymbol{k})$.

IV. ASYMPTOTIC ANALYSIS AND NUMERICAL EXPERIMENTS

A. The limit $\alpha \to 0$

In this section we will formally derive an asymptotic equation. Because $\dfrac{\partial\theta(\boldsymbol{k})}{\partial t} \to 0$ (as $\alpha \to 0$), the motion near $\alpha = 0$ takes place very slowly. To resolve such a slow motion, we may make use of the stretched time variable $\tau = \alpha t$ defined above and write

$$\frac{\partial\theta(\boldsymbol{k})}{\partial\tau} = \frac{1}{\alpha}\sum_{\boldsymbol{k}=\boldsymbol{p}+\boldsymbol{q}} \frac{\boldsymbol{p}\times\boldsymbol{q}}{|\boldsymbol{q}|^{\alpha}}\theta(\boldsymbol{p})\theta(\boldsymbol{q}). \tag{30}$$

Passing to the limit $\alpha \to 0$, we find an asymptotic equation

$$\frac{\partial\theta(\boldsymbol{k})}{\partial\tau} = \sum_{\boldsymbol{k}=\boldsymbol{p}+\boldsymbol{q}} \left(\log\frac{1}{|\boldsymbol{q}|}\right)(\boldsymbol{p}\times\boldsymbol{q})\theta(\boldsymbol{p})\theta(\boldsymbol{q}). \tag{31}$$

Note that this equation has two invariants of motion

$$Q = \frac{1}{2}\sum_{\boldsymbol{k}} |\theta(\boldsymbol{k})|^2 \text{ and } H_{\log} = \frac{1}{2}\sum_{\boldsymbol{k}} |\theta(\boldsymbol{k})|^2 \log|\boldsymbol{k}|. \tag{32}$$

At first sight, E and Q for (7) are degenerate in the limit $\alpha \to 0$, but this the apparent degeneracy is actually resolved by a logarithmic factor, as can be verified by considering $\lim_{\alpha\to 0} H_\alpha/\alpha$.

In physical space, (30) can be written

$$\frac{\partial\theta}{\partial\tau} + \frac{\partial(\psi,\theta)}{\partial(x,y)} = 0, \tag{33}$$

where the stream function is given by

$$\psi(\boldsymbol{x}) = -(\log\Lambda)\theta \equiv -\sum_{\boldsymbol{k}(\neq\boldsymbol{0})} \theta(\boldsymbol{k})\log|\boldsymbol{k}|\exp(i\boldsymbol{k}\cdot\boldsymbol{x}). \tag{34}$$

This operator is a 'derivative' of transcendentally small order, in particular, it leaves physical dimensions unchanged.

In view of the property 1), global regularity of solutions to this system is totally unknown. It remains a challenge to prove regularity because the conservation of θ controls ψ only, which is far too weak to guarantee regularity. On the other hand, in view of the property 2), this is the mildest of all the equations in the family in the sense that substantial depletion is expected in the nonlinear advection term. Recall that the nonlinear advection term is the

Jacobian of the two functions, whose physical dimensions are the same. At the moment, mathematical analysis cannot tell which factor 1) or 2) is actually dominant.Therefore we have decided to carry out some numerical simulations.

We have done some numerical experiments on the system (31), which have turned out to be difficult. This is partly because even for small τ, the motion corresponds to a very late stage in the original t. For computations we use a 2/3-dealiased pseudo-spectral method with 4096^2 grid points. Time marching is done by a fourth-order Runge-Kutta method with a time increment $\Delta t = 1 \times 10^{-4}$.

We show in Fig.2, the time evolution of contour plots of θ. As can be seen in those plots, the motion takes place slowly and deformation of the contours is very mild even at $\tau = 2.0$. However, this does not mean that θ is smooth all the time because its higher-order derivative may behave differently. For example, in Fig.3 the corresponding evolution of contour plots of 'derivative' $\Lambda\theta$ is shown. At $\tau = 2.0$ we observe steep fronts are formed in the field of $\Lambda\theta$ (see Appendix C for a note on a BKM-like criterion.) In order to estimate the strength of the (near-)singularity, we show the Fourier spectrum of θ. As expected, a power-law behavior is observed around $\tau = 1.6$ and it is close to

$$Q(k) \propto k^{-5}.$$

Note that this has a much steeper spectrum than the slope -2 the 2D Euler (or SQG) equation exhibits in the early inviscid stage.

It is an interesting question to study whether the solution breaks down at finite time or not. However, with the existing numerical data it is virtually impossible to discuss this. All we can say is that even if it does break down, the possible singularity should be much weaker than that for 2D SQG equation, that is, hiding in higher spatial derivatives.

A few more comments on the asymptotic analyses are in order. More generally, we can write by Taylor expansion,

$$\frac{\partial \theta(\boldsymbol{k})}{\partial \tau} = \sum_{n=1}^{\infty} \frac{\alpha^{n-1}}{n!} \sum_{\boldsymbol{k}=\boldsymbol{p}+\boldsymbol{q}} \left(\log \frac{1}{|\boldsymbol{q}|} \right)^n (\boldsymbol{p} \times \boldsymbol{q}) \theta(\boldsymbol{p}) \theta(\boldsymbol{q}), \tag{35}$$

or in physical space,

$$\frac{\partial \theta}{\partial \tau} + \sum_{n=1}^{\infty} \frac{\alpha^{n-1}}{n!} \frac{\partial((-\log \Lambda)^n \theta, \theta)}{\partial(x, y)} = 0, \tag{36}$$

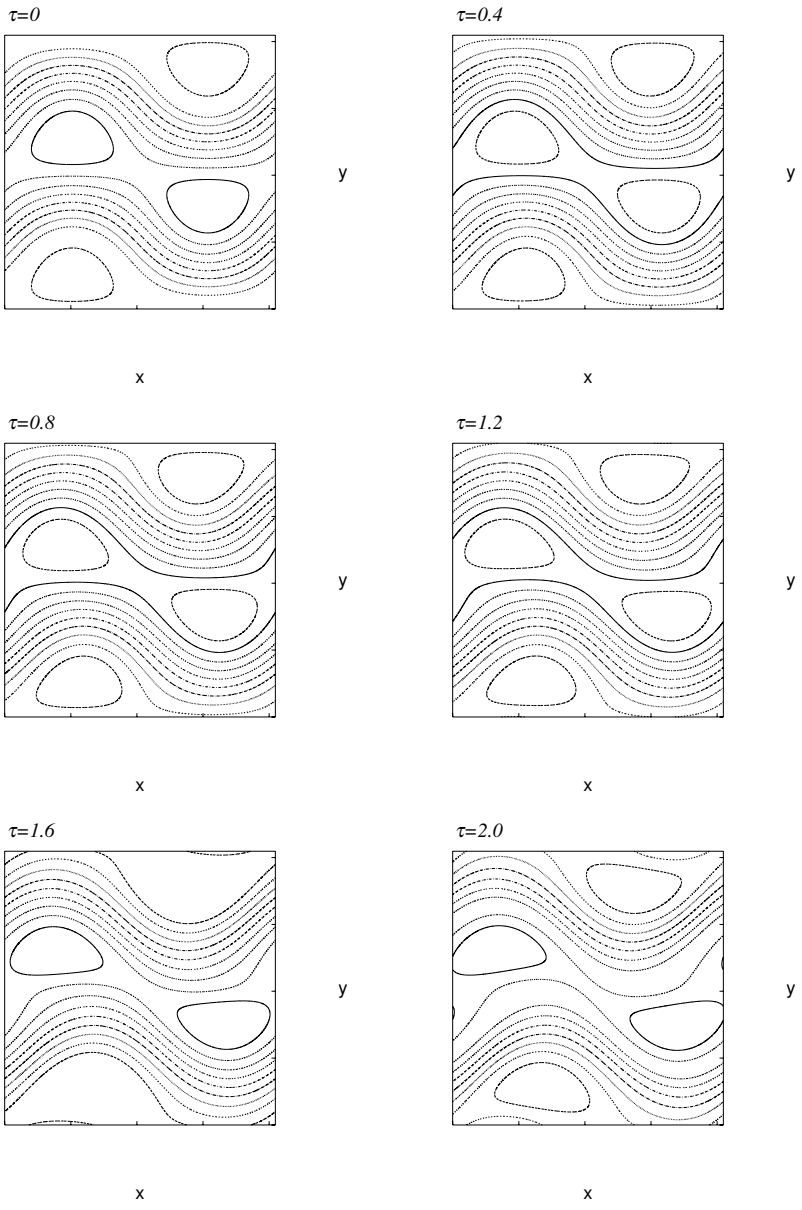

FIG. 2: Contour plots of θ for $\alpha \to 0$ at $\tau = 0, 0.4, \ldots, 2.0$. Ten equi-distant thresholds are used between the maximum and the minimum.

where

$$\psi(\boldsymbol{x}) = \Lambda^{-\alpha}\theta = \sum_{n=0}^{\infty} \frac{\alpha^n}{n!}(-\log\Lambda)^n\theta. \tag{37}$$

Note that the term $n = 0$ does not contribute in the dynamical equation (36).

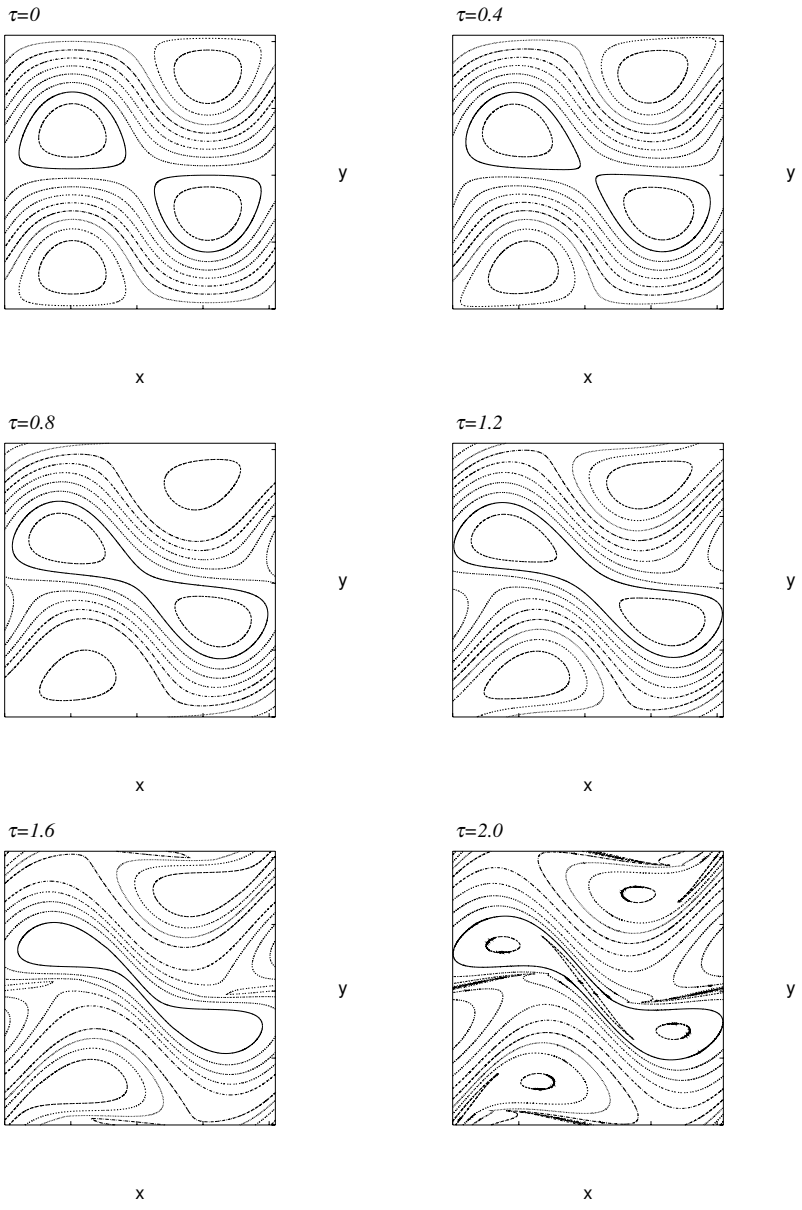

FIG. 3: Contour plots of $\Lambda\theta$ for $\alpha \to 0$ at $\tau = 0, 0.4, \ldots, 2.0$. Ten equi-distant thresholds are used between the maximum and the minimum.

It is also of interest to note that in the whole plane $\mathbb{R}^2$ the asymptotic equation (31) can be written explicitly as

$$\frac{\partial\theta}{\partial\tau} + \frac{1}{2\pi}\int\left(\frac{\partial\theta(\boldsymbol{x})}{\partial x_1}\frac{\partial\theta(\boldsymbol{x}')}{\partial x_2'} - \frac{\partial\theta(\boldsymbol{x})}{\partial x_2}\frac{\partial\theta(\boldsymbol{x}')}{\partial x_1'}\right)\frac{\boldsymbol{dx'}}{|\boldsymbol{x}-\boldsymbol{x}'|^2} = 0. \tag{38}$$

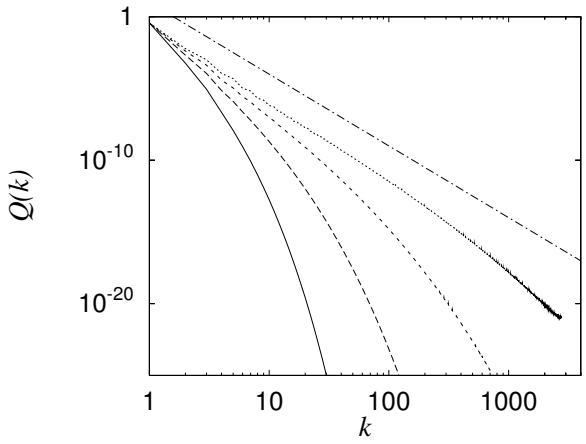

FIG. 4: Evolution of spectra of θ for $\alpha \to 0$ at $\tau = 0.4, 0.8, 1.2, 1.6$, from left to right. The dashed line denotes a slope of k^{-5}.

We note that an apparent singularity of the kernel at $\boldsymbol{x} = \boldsymbol{x}'$ is harmless, as the (two-point) Jacobian-like factor vanishes there. It is also noted that a logarithmic contribution is hidden in $\dfrac{\boldsymbol{dx'}}{|\boldsymbol{x} - \boldsymbol{x}'|^2} \propto \dfrac{dr}{r} = d \log r$. Care should be taken as the splitting the integrand in two parts would lead to a result which does not make any sense, i.e. divergent integrals.

B. Numerics for the limit $\alpha \to 2$

The first variation $\theta_1(\boldsymbol{k}) \equiv \frac{\partial \theta(\boldsymbol{k})}{\partial \alpha}$ at $\alpha = 2$ is governed by

$$\frac{\partial \theta_1(\boldsymbol{k})}{\partial t} = \sum_{\boldsymbol{k}=\boldsymbol{p}+\boldsymbol{q}} \frac{\boldsymbol{p} \times \boldsymbol{q}}{|\boldsymbol{q}|^\alpha} \left(\theta_1(\boldsymbol{p})\omega(\boldsymbol{q}) + \omega(\boldsymbol{p})\theta_1(\boldsymbol{q}) + \omega(\boldsymbol{p})\omega(\boldsymbol{q}) \log \frac{1}{|\boldsymbol{q}|} \right), \tag{39}$$

where the initial condition was taken to be $\theta_1(\boldsymbol{k}) = 0$. This describes principal variation near the 2D Euler limit of $\alpha = 2$. We have numerically solved this equation together with the 2D Euler equations. The initial condition for the variation is $\theta_1 = 0$ and it becomes non-zero by the final term of the right-hand-side of (39).

We show in Fig.5 the time evolution of contours of the vorticity. As usual, we observe formation of steep gradients of vorticity. In Fig.6 we show corresponding contour plots for θ_1. It should be noted that the principal variation has characteristic structures near the steep vorticity gradients in the central region.

Next, we study the spectral properties of these fields. We show in Fig.7 the evolution of

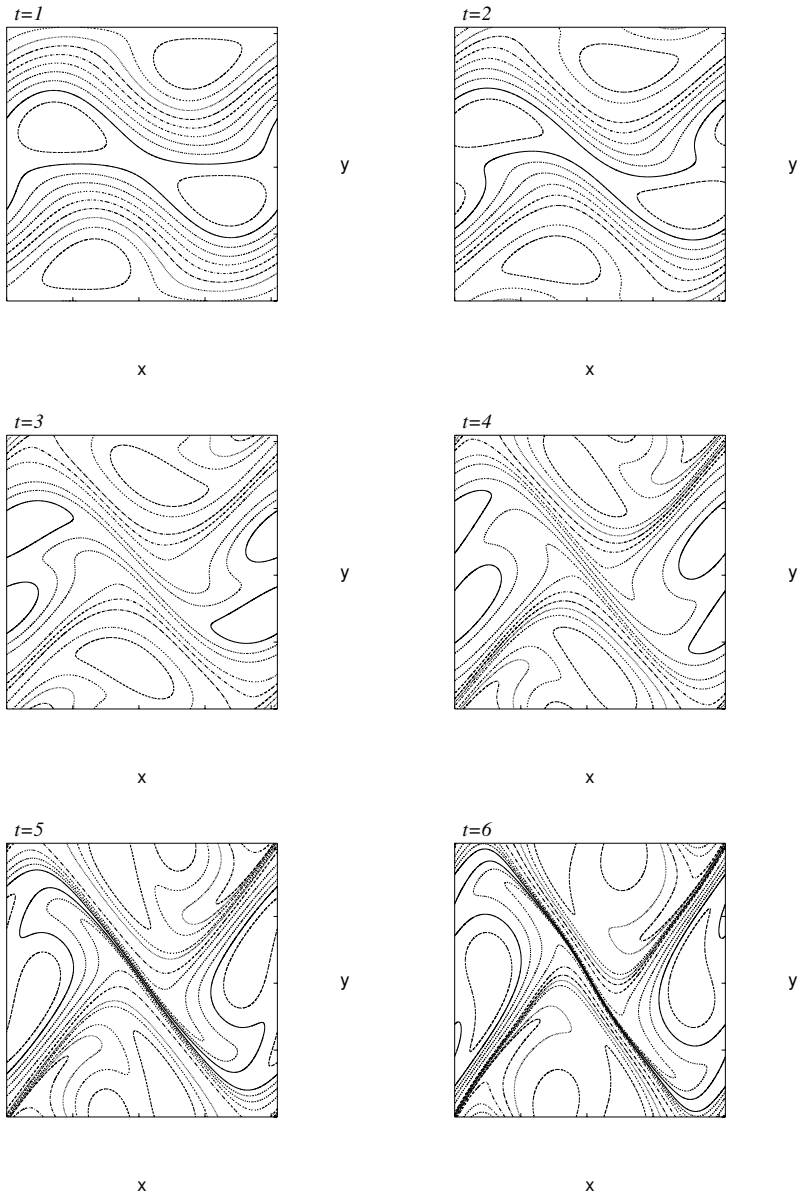

FIG. 5: Contour plots of θ for $\alpha = 2$ (2D Euler) at $t = 1, 2, \ldots, 6$, plotted as in Fig.2.

enstrophy spectra, which is at late times close to

$$Q(k) \propto k^{-2}. \tag{40}$$

This is consistent with the well-known Saffman's model expected to hold in the inviscid stage [18].

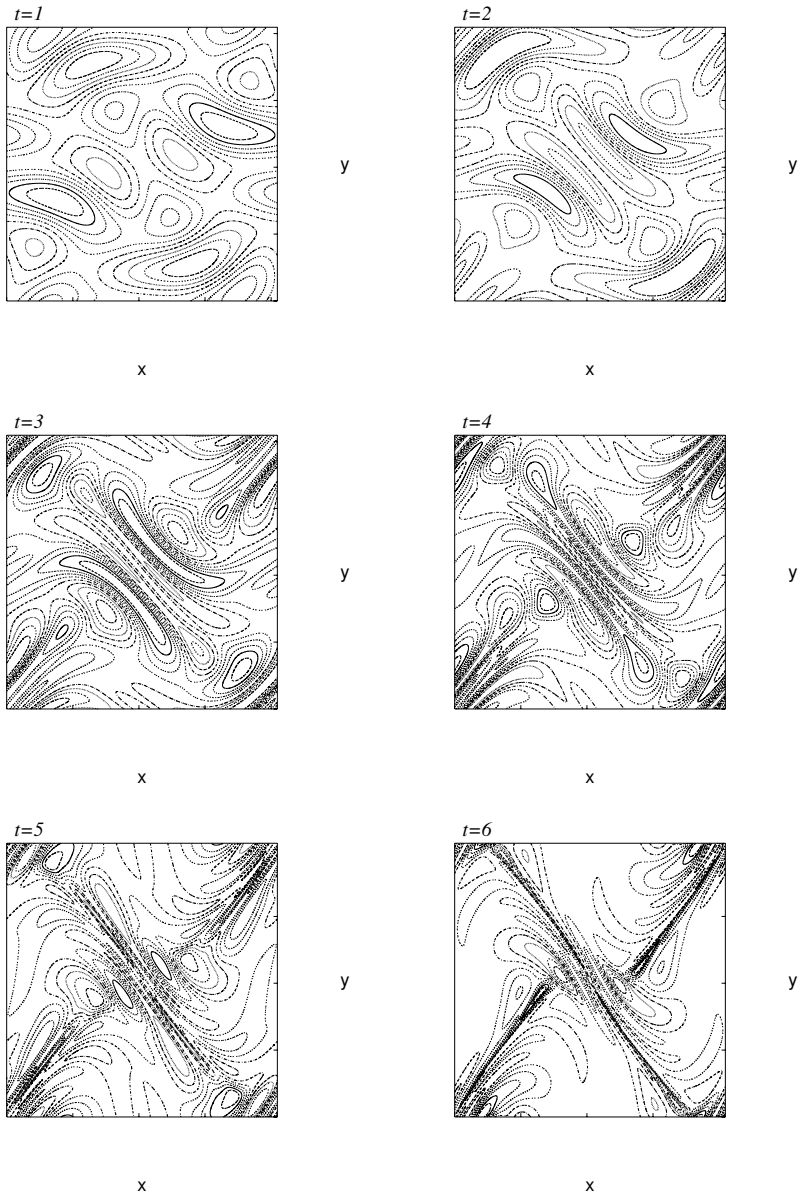

FIG. 6: Contour plots of the principal variation θ_1 for $\alpha = 2$ (2D Euler) at $t = 1, 2, \ldots, 6$, plotted as in Fig.2.

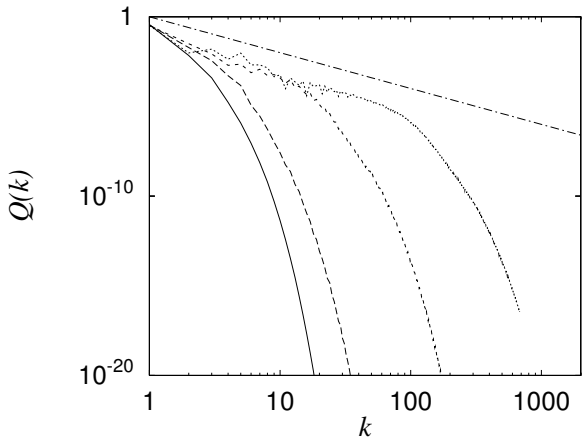

FIG. 7: Evolution of spectra $Q(k)$ of θ for $\alpha = 2$ at $t = 1, 2, 4$ and 6, from left to right. The dashed line denotes a slope of k^{-2}.

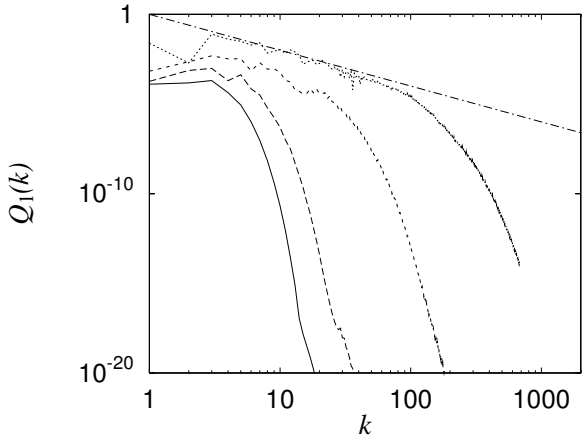

FIG. 8: Evolution of spectra $Q_1(k)$ of the principal variation θ_1 for $\alpha = 2$ at $t = 1, 2, 4$ and 6, from left to right. The dashed line denotes a slope of k^{-2}.

We also show the time evolution of the Fourier spectrum of the variational field in Fig.8. Again we find that its spectrum is close to

$$Q_1(k) \propto k^{-2}, \tag{41}$$

that is, the slope is the same as that of the vorticity field. At the moment we have no explanation why these slopes should identical and the coincidence may be accidental.

V. NUMERICAL EXPERIMENTS FOR OTHER α

A. Case of $\alpha = 0.5$

The limit of $\alpha \to 0$ corresponds to examining the flow in its very late stage of development in the original t. Special care should be needed to carry out reliable computations in the choice of time step and spatial resolutions. We compare the cases of $\alpha = 0.5$ and $\alpha \to 0$ in Figs.9. They turned out to be similar to each other as long as the contour plots are concerned. It is of interest to compare the time evolution of the active scalar with different α's at the same τ.

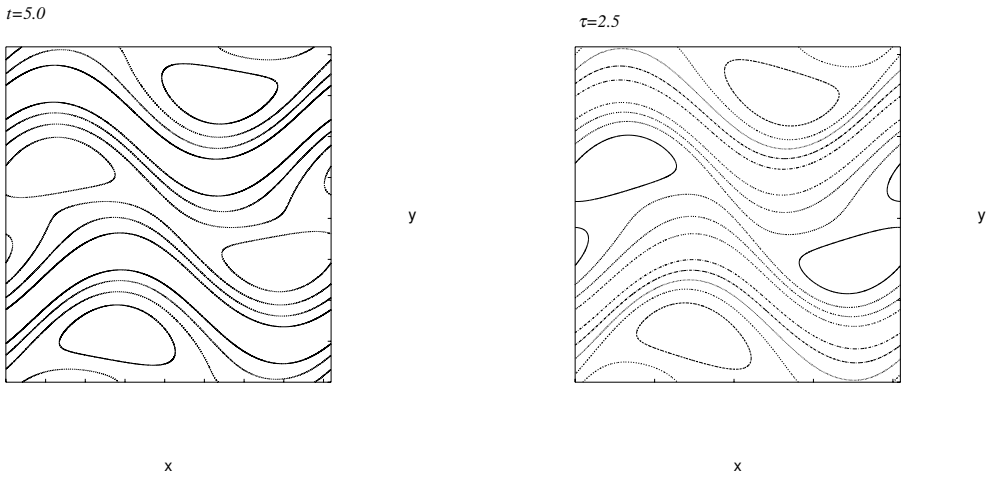

FIG. 9: Contour plot of θ: for $\alpha = 0.5$ at $t = 5.0$ corresponding to $\tau = 2.5$ (left) and for $\alpha \to 0$ at $\tau = 2.5$ (right).

B. Cases of $\alpha = 1, 1.5, 2$

We compare the time evolution of the active scalar in the range $\alpha \geq 1$. In the previous study, we have compared the time evolution of contour plots of θ for $\alpha = 1, 1.5$ and 2 at fixed t's, see figures 10-12 in [13]. We have observed marked different behaviors in their patterns. Here we will compare them at fixed τ's. In Figs.10 we show the contour plots at

$\tau = 6.0$. We see the patterns look similar to each other, particularly the inclination of of the thin layers being formed in the central region. In Figs.11, we likewise compare those fields at $\tau = 9.0$. Again we see that the patterns look quite similar to each other. Actually, despite the similarity in the pattern, norms take markedly different values (see below).

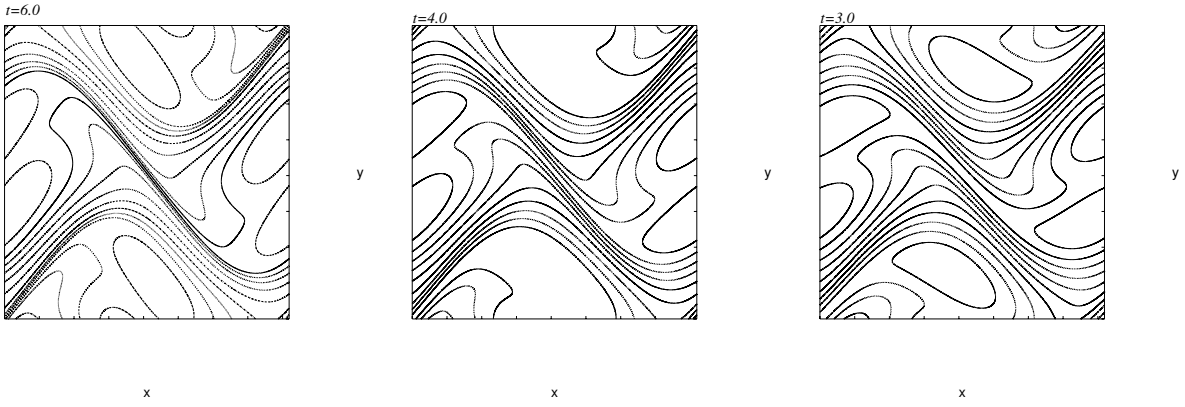

FIG. 10: Contour plots at $\tau = 6.0$: (left) $\alpha = 1$(SQG), $t = 6.0$, (middle) $\alpha = 1.5$, $t = 4.0$, and (right) $\alpha = 2.0$(2D Euler), $t = 3.0$, from left to right.

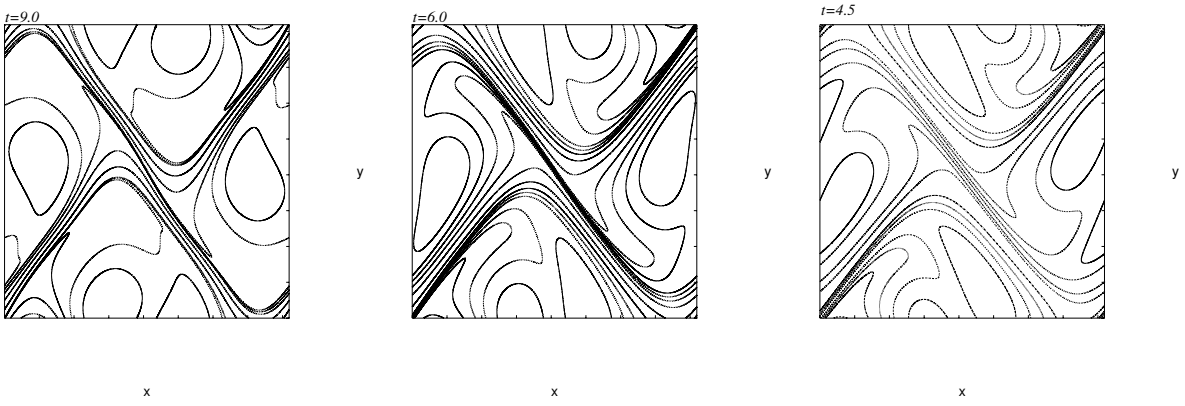

FIG. 11: Contour plots at $\tau = 9.0$: (left) $\alpha = 1$(SQG), $t = 9.0$, (middle) $\alpha = 1.5$, $t = 6.0$, and (right) $\alpha = 2.0$(2D Euler), $t = 4.5$, from left to right.

We next examine the time evolution of scalar gradient by

$$P(t) = \frac{1}{2}\left\langle |\nabla\theta|^2 \right\rangle,$$

which is essentially the H_1 norm of θ in Figs.12. We also show the case of $\alpha = 0.5$ for comparison. As we can see, generally speaking, $P(t)$ grows faster with increasing α except for the late stage.

However, if we plot the same thing using $\tilde{P}(\tau) = P(t)$ with $\tau = \alpha t$, the evolution looks completely different, that is, the order is reversed; $\tilde{P}(\tau)$ grows faster with *decreasing* α. See Fig.12 where we have included $\alpha = 0.5$ and $\alpha \to 0$ as well.

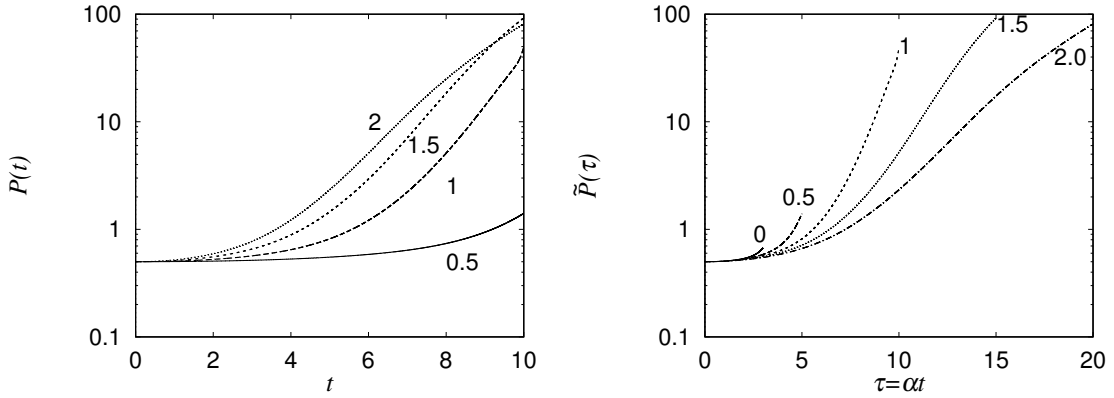

FIG. 12: Evolution of $P(t)$ (left) and $\tilde{P}(\tau)$ (right) for several α's.

The formal asymptotics may be valid only for small values of α, because it relies on a series expansion. However, the observed similarity in contour plots suggests that such a connection between different α's may still hold beyond the validity of series analysis.

To check this view quantitatively, we compute a correlation coefficient between ω for the 2D Euler equations and θ for the generalized SQG equations

$$C_\alpha = \frac{\int \omega(\boldsymbol{x},t)\theta(\boldsymbol{x},t;\alpha)\boldsymbol{dx}}{\sqrt{\int \omega(\boldsymbol{x},t)^2\boldsymbol{dx}\int \theta(\boldsymbol{x},t;\alpha)^2\boldsymbol{dx}}},$$

for $\alpha = 1$ and 1.5, using both t and τ. Recall that $\theta(\boldsymbol{x},t;\alpha=2) \equiv \omega(\boldsymbol{x},t)$. In Fig.13 we show the correlations for $\alpha = 1$ and 1.5 using both t and τ. With the original time t, the correlation drops at $t = 8$ by 10% for $\alpha = 1.5$ and 20 % for $\alpha = 1$. With the new time τ the correlation decays by less than 5% for both values of α. On the time τ, the correlations decay more slowly than on t, even at no so small α as 1 and 1.5.

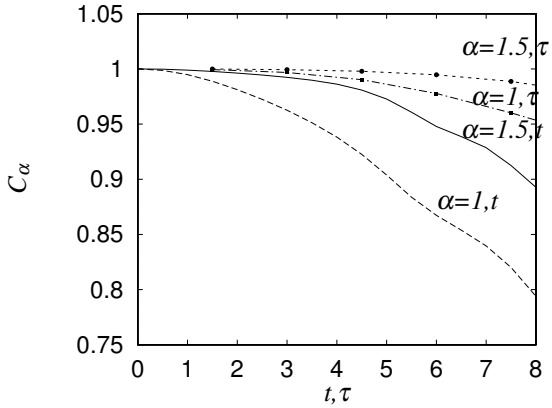

FIG. 13: The correlation coefficient C_α, plotted against t and τ for $\alpha = 1, 1.5$.

VI. SUMMARY AND OUTLOOK

In order to study how the SQG equation is similar to, or different from the 2D Euler equation, we have considered perturbations of the generalized SQG equations. An expansion from the steady state ($\alpha = 0$) is studied together with that from the 2D Euler equation ($\alpha = 2$). Two mechanisms of regularization are identified: near $\alpha = 0$ (complete depletion) as α increases the solution becomes more singular, whereas near $\alpha = 2$ (maximal smoothing effect of inverse Laplacian) as α decreases the solution becomes more singular. This suggest that there may be some α in $[0, 1]$ at which the solution is most singular.

By introducing the scaled time variable $\tau = \alpha t$ we attempt to unify generalized equations in the limit of $\alpha \to 0$. limit. Numerical experiments suggest that even for not so small α, all contour plots of θ look similar when compared at the same values of τ. An asymptotic equation is derived ($\alpha \to 0$), whose numerics suggests that $Q(k) \propto k^{-5}$. This indicates that if a singularity is present, it is in higher-order derivatives such as $\nabla^2\theta$, and not in $\nabla\theta$.

It may be of interest to treat the recursion relationship (29) numerically and compare with direct numerical simulations.

Acknowledgments

This work has been partially supported by an EPSRC grant EP/F009267/1. The author has been supported by Royal Society Wolfson Research Merit Award. Part of this work has been presented at a Conference "Dissipative PDEs in Bounded and Unbounded Domains and Related Attractors" at ICMS, Edinburgh in September 2010. The author thanks P.

Constantin and T. Sakajo for discussion.

APPENDIX A: POINCARÉ'S PERTURBATION THEORY FOR ODES

(Notations used here are independent from the rest of the paper.)
We consider an ODE with a parameter μ e.g. [20]

$$\frac{dy}{dx} = f(x, y, \mu), \text{ with } y(x_0, \mu) = y_0. \tag{A1}$$

The variation defined by

$$z(x, \mu) = \frac{\partial y(x, \mu)}{\partial \mu}, \text{ with } z(x_0, \mu) = 0 \tag{A2}$$

satisfies

$$\frac{dz}{dx} = \left.\frac{\partial f(x, Y, \mu)}{\partial Y}\right|_{Y=y(x,\mu)} z + \left.\frac{\partial f(x, Y, \mu)}{\partial \mu}\right|_{Y=y(x,\mu)}, \tag{A3}$$

which is called équation aux variations. Assuming that we have a solution $y(x)$ to

$$\frac{dy}{dx} = f(x, y, \mu_0), \text{ with } y(x_0, \mu_0) = y_0, \tag{A4}$$

we solve

$$\frac{dY(x, \mu)}{dx} = f(x, Y, \mu), \text{ with } Y(x_0) = y_0 \tag{A5}$$

approximately for small $|\mu - \mu_0|$. By analyticity assumption we write

$$y(x, \mu) - y(x, \mu_0) = \sum_{n=1}^{\infty} (\mu - \mu_0)^n C_n(x) \tag{A6}$$

and the principal term is given by

$$z(x, \mu_0) = \lim_{\mu \to \mu_0} \frac{y(x, \mu) - y(x, \mu_0)}{\mu - \mu_0} = C_1(x). \tag{A7}$$

APPENDIX B: LAGRANGIAN REPRESENTATION

A system of point-vortices for the SQG was studied e.g. in [21]. We may consider a system of N point-vortices for the generalized SQG equations:

$$\frac{dx_i}{dt} = \frac{\alpha - 2}{\gamma(\alpha)} \sum_{j=1}^{N} \kappa_j \frac{y_i - y_j}{((x_i - x_j)^2 + (y_i - y_j)^2)^{(4-\alpha)/2}}, \tag{B1}$$

$$\frac{dy_i}{dt} = -\frac{\alpha-2}{\gamma(\alpha)}\sum_{j=1}^{N}\kappa_j \frac{x_i - x_j}{((x_i-x_j)^2+(y_i-y_j)^2)^{(4-\alpha)/2}} \tag{B2}$$

$(i = 1 \ldots N)$. For the case of a vortex pair ($N = 2$), there are known solutions which propagate at a constant speed if κ's are oppositely signed, or rotate around the center of gravity at a constant angular velocity.

More precisely, if $\kappa_1 = -\kappa_2 = \kappa(> 0)$ a pair which is at a distance d propagates at a speed

$$v = \frac{2-\alpha}{\gamma(\alpha)}\frac{\kappa}{d^{3-\alpha}}.$$

On the other hand, if $\kappa_1, \kappa_2 > 0$, a pair rotates at an angular velocity

$$\Omega = \frac{2-\alpha}{\gamma(\alpha)}\frac{\kappa_1+\kappa_2}{d^{4-\alpha}}.$$

We introduce a function

$$F(\alpha) = \pi\frac{2-\alpha}{\gamma(\alpha)}d^\alpha = (2-\alpha)\left(\frac{d}{2}\right)^\alpha \frac{\Gamma(1-\alpha/2)}{\Gamma(\alpha/2)},$$

which represents a characteristic frequency (velocity) for the "vortex pair" in the generalized QG model. This depends on d. As we are interested in small-scale excitation $d < 1$ we plot $F(\alpha)$ as a function of α for the two examples of $d = 1/4$ and $d = 1/2$. They attain a maximum between $0 < \alpha < 1$. This is a rough qualitative test, but it suggests that most singular parameter lies somewhere in the middle.

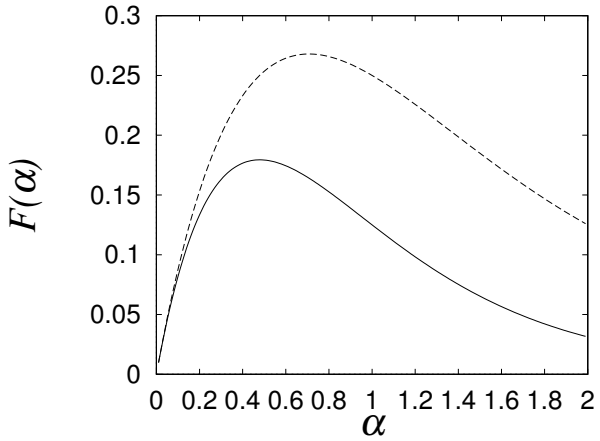

FIG. 14: The function $F(\alpha)$; for $d = 1/4$(solid) and $d = 1/2$ (dashed).

APPENDIX C: NOTE ON BKM-TYPE CRITERION

The BKM-type criterion [22] is well- known for the existence of smooth solutions of the 3D Euler equations. This was extended by [23] using BMO-norm.

It is also possible to work out such a criterion for the SQG system ($\alpha = 1$) [24]. We point out that for the generalized system such an estimate is available for $\alpha \geq 1$ using L^∞(or BMO) norm of $\nabla\theta$.

Using a standard commutator estimate [25, 26]

$$\|\Lambda^s(fg) - f\Lambda^s g\|_{L^2} \leq C\left(\|\nabla f\|_{\rm BMO}\|g\|_{s-1} + \|f\|_{s-1}\|\nabla g\|_{\rm BMO}\right), \tag{C1}$$

where $\|\cdot\|_s$ denotes a Sobolev norm of order s. By taking $f = u, g = \nabla\theta$, we obtain

$$\frac{d\|\theta\|_s}{dt} \leq C\left(\|\nabla u\|_{\rm BMO}\|\theta\|_s + \|\nabla\theta\|_{\rm BMO}\|u\|_s\right). \tag{C2}$$

When $\alpha \geq 1$, θ has got a higher derivative than $\boldsymbol{u}$ and we conclude

$$\frac{d\|\theta\|_s}{dt} \leq C\|\nabla\theta\|_{\rm BMO}\|\theta\|_s, \tag{C3}$$

from which a BMO-extended BKM type criterion

$$\int_0^T \|\nabla\theta\|_{\rm BMO}(t)dt < \infty \tag{C4}$$

follows for smooth existence on a time interval $[0, T)$. On the other hand, if $\alpha < 1$, it is $\boldsymbol{u}$ that has a higher derivative and we have

$$\frac{d\|\theta\|_s}{dt} \leq C\|\nabla u\|_{\rm BMO}\|\theta\|_{s+1-\alpha}. \tag{C5}$$

(Note in this case $\|u\|_s = \|\theta\|_{s+1-\alpha}$.) We may need a higher derivative e.g. $\nabla^2\theta$ to get a suitable criterion.

---

[1] P. Constantin, A.J. Majda and E. Tabak, "Formation of strong fronts in the 2-D quasi-geostrophic thermal active scalar," Nonlinearity **7**, 1495(1994).

[2] P. Constantin, A.J. Majda and E. Tabak, "Singular front formation in a model for quasi-geostrophic flow," Phys. Fluids **6**, 9 (1994).

[3] P. Constantin, "Geometric statistics in turbulence," SIAM Review **36**, 73(1994).

[4] A.J. Majda and E. Tabak, "A two-dimensional model for quasigeostrophic flow: comparison with the two-dimensional Euler flow," Physica D **98**, 515(1996).

[5] K. Ohkitani and M. Yamada, "Inviscid and inviscid-limit behavior of a surface quasi-geostrophic flow," Phys. Fluids, **9**, 876(1997).

[6] P. Constantin, Q. Nie and N. Schörghofer, "Nonsingular surface quasi-geostrophic flow," Phys. Lett. A **241**, 168(1998).

[7] J. Deng, T.Y. Hou, R. Li and X. Yu, "Level Set Dynamics and the Non-blowup of the 2D Quasi-geostrophic Equation," Methods Appl. Anal. **13**, 157(2006).

[8] P. Constantin, "Singular, weak and absent: Solutions of the Euler equations," Physica D **237** 1926(2008).

[9] P. Constantin, M.-C. Lai, R. Sharma, Y.-H. Tseng and J. Wu, "New numerical results for the surface quasi-geostrophic equation," J. Sci. Comput. **50**, 1 (2012).

[10] A. Kiselev, F. Nazarov and A. Volberg, "Global well-posedness for the critical 2D dissipative quasi-geostrophic equation," Invent. Math. **167**, 445(2007).

[11] L. Caffarelli and A. Vasseur, "Drift diffusion equations with fractional diffusion and the quasi-geostrophic equation," to appear in Acta Math.

[12] C.V. Tran, D.G. Dritschel and R.K. Scott, "Effective degrees of nonlinearity in a family of generalized models of two-dimensional turbulence," Phys. Rev. E **81**, (2010) 016301-1.

[13] K. Ohkitani, "Growth rates analysis of scalar gradient in generalized surface quasi-geostrophic equations of ideal fluids," Phys. Rev. E **83**, 036317-1(2011).

[14] D. Chae, P. Constantin and J. Wu, "Inviscid models generalizing the 2D Euler and the surface quasi-geostrophic equations," Arch. Rat. Mech. Anal. **202**, 35 (2011).

[15] D. Chae, P. Constantin and J. Wu, "Dissipative models generalizing the 2D Navier-Stokes and the surface quasi-geostrophic equations," arXiv:1011.0171, (2010).

[16] D Chae, P Constantin, D Cordoba, F Gancedo and J. Wu, "Generalized surface quasi-geostrophic equations with singular velocities," arXiv:1101.3537, (2011).

[17] C.V. Tran and J.C. Bowman, "Energy budgets in Charney-Hasegawa-Mima and surface quasi-geostrophic turbulence," Phys. Rev. E **68**, 036304-1(2003).

[18] P.G. Saffman, "On the spectrum and decay of random two-dimensional vorticity distributions at large Reynolds number," Stud. Appl. Math. **50**, 377(1971).

[19] E.M. Stein, *Harmonic Analysis: Real-Variable Methods, Orthogonality, and Oscillatory Inte-*

grals, (Princeton University Press, Princeton, 1993).

[20] K. Yosida, *Lectures on Differential and Integral Equations,* (John Wiley & Sons Inc, New York, 1960).

[21] S. Hoshi and T. Miyazaki, "Statistics of quasi-geostrophic point vortices," Fluid Dyn. Res. **40**, 662 (2008).

[22] J.T. Beale, T. Kato and A. Majda, "Remarks on the breakdown of smooth solutions for the 3D Euler equations," Commun. Math. Phys. **94**, 61(1984).

[23] H. Kozono and Y. Taniuchi, "Limiting case of the Sobolev inequality in BMO, with application to the Euler equations, Comm. Math. Phys. **214**, 191 (2000).

[24] N. Ju, "The 2D quasi-geostrophic equations in the Sobolev space," in *Harmonic analysis, partial differential equations and related topics,* ed. E.A. Gavosto, Contemporary Mathematics **428**(2007) pp.75–92.

[25] R.R. Coifman and Y. Meyer, Au delá des opérateurs pseudo-différentiels, Astérisque **57** (1978).

[26] R.R. Coifman and Y. Meyer, Nonlinear harmonic analysis, operator theory and P.D.E., in *Beijing Lectures in Harmonic Analysis,* ed. E.M. Stein, (Princeton University Press, Princeton, 1986).